INTERNATIONAL JOURNAL OF CLIMATOLOGY
Int. J. Climatol. **34**: 1062–1080 (2014)
Published online 18 June 2013 in Wiley Online Library
(wileyonlinelibrary.com) DOI: 10.1002/joc.3746

Royal Meteorological Society

Evaluation of the 'local climate zone' scheme using temperature observations and model simulations

Iain D. Stewart,* T. R. Oke and E. Scott Krayenhoff

Department of Geography, University of British Columbia, Vancouver, BC, Canada V6T 1Z2,

ABSTRACT: 'Local climate zones' (LCZs) comprise a new and systematic classification of field sites for heat island studies. The classification divides urban and rural landscapes into 17 standard classes, each defined by structural and land cover properties that influence air temperature at screen height. This study is the first to evaluate the conceptual division of LCZs with temperature observations and simulation results from surface–atmosphere models. Results confirm that thermal contrasts exist among all LCZ classes, and that such contrasts are governed largely by building height and spacing, pervious surface fraction, tree density, and soil wetness. Therefore, partitioning of landscapes into structural and land cover classes, or 'LCZs,' is deemed justified for the purposes of field site classification in heat island studies. Also justified is the use of inter-zone temperature difference ($\Delta T_{\mathrm{LCZ\ X-Y}}$) to quantify heat island magnitude. To further improve the LCZ system, we encourage other researchers to observe and model the climatic conditions of its varied classes. Especially useful would be tests using field data from different urban and rural environments to those in this study, and running more advanced urban canopy models with demonstrated predictive capability.

KEY WORDS local climate zones; canopy-layer air temperature; urban heat island; site classification; field observations; model simulations

Received 20 July 2012; Revised 3 April 2013; Accepted 21 April 2013

1. Introduction

Urban climatology is a rapidly growing field. Standards are therefore necessary to ensure consistent and meaningful exchange of data across regions, cultures, and disciplines. The adoption of common scales, symbols, techniques, and terminology could enable urban climatologists to communicate more effectively (Oke, 2006). One area of standardization that has hardly advanced is the classification of field sites for urban heat island (UHI) studies. The traditional approach has been to designate sites in the city and countryside as 'urban' and 'rural,' with little attention given to the local or micro-scale character of those sites. In practice, investigators rarely report the site metadata necessary to quantify or otherwise elucidate the terms 'urban' and 'rural' (Stewart, 2011a). Uncritical use of these terms in the heat island literature has caused unnecessary confusion around the actual exposure and land cover conditions of field sites.

The 'local climate zone' (LCZ) classification recently developed by Stewart and Oke (2012) specifically addresses problems of method and communication in heat island studies. The primary aim of the system is to facilitate consistent and climatologically relevant classifications of urban and rural field sites for temperature observations at standard screen height (1–2 m above ground). The system comprises 17 standard classes at the local scale (10^2 to 10^4 m) (Figure 1). Each class is unique in its combination of surface structure (building/tree height and spacing), cover (pervious fraction), fabric (albedo, thermal admittance), and metabolism (anthropogenic heat flux). When compared under similar atmospheric and surface relief conditions, each LCZ should portray a characteristic air temperature regime at screen height. LCZs are individually named and ordered by one (or more) distinguishing surface property, which for most classes is land cover or the height/spacing of trees and buildings. The surface properties of all zones are measurable and non-specific as to time or place (Table 1).

Operational guidelines and recommended uses for LCZs are provided in Stewart and Oke (2012). There it is shown that the system is derived conceptually from structural division of the urban–rural landscape into local-scale units. What are not shown are climatological data to support that division. This study provides the first such data in the form of temperature observations from three representative cities located in Western Europe, East Asia, and North America, and simulation results from surface–atmosphere numerical models.

2. Observational approach

2.1. Study sites and methods

To differentiate the thermal climates of LCZ classes, we acquired screen-level temperatures from heat island

* Correspondence to: I. D. Stewart, Department of Geography, University of British Columbia, 1984 West Mall, Vancouver, BC, Canada V6T 1Z2. E-mail: stewarti@interchange.ubc.ca

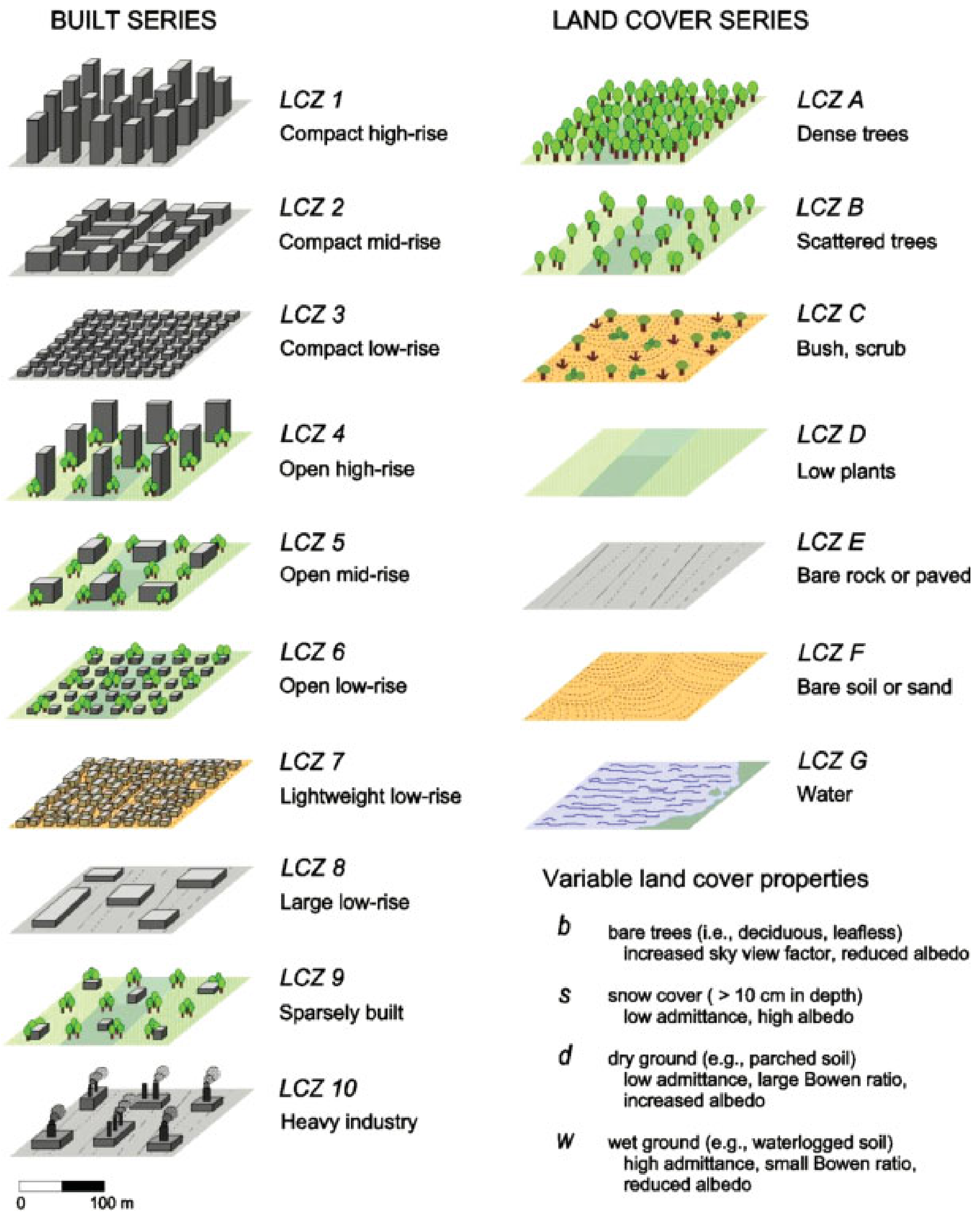

Figure 1. The 'local climate zone' (LCZ) classification scheme and its 17 standard classes. The convention to create subclasses and assign variable land cover properties (e.g. *wet ground*, *snow cover*) is given in Stewart and Oke (2012).

studies in Nagano, Japan (36°N, 138°E); Vancouver, Canada (49°N, 123°W); and Uppsala, Sweden (59°N, 17°E). These cities were chosen because they offer different cultural, historical, climatic, and geographic settings in which to investigate the effects of urban form, rural soil wetness, tree density, snow cover, and human activity on LCZ temperatures. They also offer high-quality observations that meet the four criteria of good scientific practice in heat island studies suggested by Stewart (2011a), viz: (1) urban and non-urban effects (e.g. weather, surface relief, non-synchronous measurement) on air temperature are suitably controlled for through experimental design, data selection, and/or data correction; (2) the source areas of field sites are reasonably uniform and thus able to be easily classified; (3) site metadata are appropriately detailed; and (4) instruments are properly sited and mounted for heat island measurement in the canopy layer (i.e. below roof level). Further details of the observations, including site maps and photographs, are provided in the original reports of Sakakibara (1999), Sakakibara and Matsui (2005), Sundborg (1951), and Taesler (1980). A summary of these reports and of the unpublished datasets used in this study for Nagano, Vancouver, and Uppsala is given in Stewart (2011b).

The weather factor (Φ_W) of Oke (1998) was used to identify relatively calm, clear nights suitable for the development of local climates. Φ_W is derived from nonlinear relations between UHI magnitude and cloud and wind conditions:

$$\Phi_W = u^{-1/2}\left(1 - kn^2\right)$$

Table 1. Simplified table of surface property values for local climate zones (*Source*: Stewart and Oke, 2012).

Local climate zone (LCZ)	Aspect ratio[a]	Sky view factor[b]	Building surface fraction[c]	Impervious surface fraction[d]	Height of roughness elements[e]	Anthropogenic heat flux density[f]
LCZ 1 Compact high-rise	>2	0.2–0.4	40–60	40–60	>25	50–300
LCZ 2 Compact mid-rise	0.75–1.5	0.3–0.6	40–70	30–50	8–20	<75
LCZ 3 Compact low-rise	0.75–1.5	0.2–0.6	40–70	20–40	3–8	<75
LCZ 4 Open high-rise	0.75–1.25	0.5–0.7	20–40	30–40	>25	<50
LCZ 5 Open mid-rise	0.3–0.75	0.5–0.8	20–40	30–50	8–20	<25
LCZ 6 Open low-rise	0.3–0.75	0.6–0.9	20–40	20–40	3–8	<25
LCZ 7 Lightweight low-rise	1–2	0.2– 0.5	60–90	<10	2–4	<35
LCZ 8 Large low-rise	0.1–0.3	>0.7	30–50	40–50	3–10	<50
LCZ 9 Sparsely built	0.1–0.25	>0.8	10–20	<20	3–8	<10
LCZ 10 Heavy industry	0.2–0.5	0.6–0.9	20–30	20–40	5–15	>300
LCZ A Dense trees	>1	<0.4	<10	<10	3–30	0
LCZ B Scattered trees	0.25–0.75	0.5–0.8	<10	<10	3–15	0
LCZ C Bush, scrub	0.25–1.0	>0.9	<10	<10	<2	0
LCZ D Low plants	<0.1	>0.9	<10	<10	<1	0
LCZ E Bare rock or paved	<0.1	>0.9	<10	>90	<0.25	0
LCZ F Bare soil or sand	<0.1	>0.9	<10	<10	<0.25	0
LCZ G Water	<0.1	>0.9	<10	<10	—	0

[a]Mean height-to-width ratio of street canyons (LCZs 1–7), building spacing (LCZs 8–10), and tree spacing (LCZs A–G).
[b]Ratio of the amount of sky hemisphere visible from ground level to that for an unobstructed hemisphere.
[c]Proportion of ground surface with building cover (%).
[d]Proportion of ground surface with impervious cover (rock, paved) (%).
[e]Geometric average of building heights (LCZs 1–10) and tree/plant heights (LCZs A–F) (m).
[f]Mean annual anthropogenic heat flux density ($W\,m^{-2}$) at the local scale. Varies significantly with latitude, season, and population density.

where $u^{-1/2}$ is an empirical relation between heat island magnitude and regional wind speed ($m\,s^{-1}$) (Oke, 1973), and $1 - kn^2$ is the Bolz correction for net longwave radiation under a given cloud type (k) and cloud amount (n) (Bolz, 1949). Φ_W expresses the degree to which wind and sky conditions permit nocturnal cooling of the near surface layer. Strictly, Φ_W has units, but it is treated as a non-dimensional number able to indicate relative cooling potential. Values range from 0 (poor cooling, no heat island effect) to 1 (excellent cooling, maximum heat island effect). Because of its square root form, the relation is limited to wind speeds $>1\,m\,s^{-1}$, which becomes the default value in calm or near-calm conditions. The selection criterion for nights used in this study was $\Phi_W \geq 0.7$, with no precipitation in the preceding 24 h.

Metadata for observation sites in the three cities were gathered according to guidelines in Aguilar *et al.* (2003), Oke (2004), and Stewart and Oke (2012). The approximate source areas for the sites were represented by physical surface properties that define LCZs (Table 1). In dense urban surroundings (e.g. city core), source areas were set to encompass a 100 m radius from the site; in more open fetch (e.g. city outskirts), they cover a radius of 200 m. The distance at urban stations is based on empirical evidence that suggests source areas for screen-height thermometres in neutrally stable atmospheres extend no more than a few hundred metres away (Tanner, 1963; Mizuno *et al.*, 1990/91; Runnalls and Oke, 2006). The larger distance for rural sites accounts for greater stability, which reduces turbulent activity. LCZ classes that best matched the measured or estimated surface properties of the source areas were then selected. To facilitate this process, metadata were retrieved from Google Earth© images, historical maps and photographs, and site visits by the authors to the three cities including interviews with the original heat island investigators.

2.1.1. Nagano, Japan

Nagano is an expansive city (population 300 000) located in a broad, interior valley with a humid subtropical climate. Temperature data were obtained from Sakakibara and Matsui (2005), who conducted 90 evening traverses across the surrounding basin to capture the seasonal effects of land cover change on screen-height temperatures. All measurements were made between 2200 and 0200 hours, with a thermistor probe (precision ± 0.2 K) mounted 1.5 m above ground and attached to the roof of a car. Ancillary cloud, wind, and precipitation data for the 90 traverses, each lasting about 75 min, were extracted from standard meteorological records at Nagano Local Observatory. These data were used to identify evenings that met the selection criterion (i.e. $\Phi_W \geq 0.7$, no precipitation). The observation sites selected along the traverse route were classified into LCZs using field site metadata and the heat island reports of Sakakibara (1999) and Sakakibara and Matsui (2005).

Supplementary temperature data were obtained from three fixed stations in and around the town of Obuse (population 10 000), an agricultural community 12 km northeast of Nagano city. The stations recorded hourly air temperatures from July 2006 to June 2007 (Sakakibara, unpublished). Each station housed a Hobo thermistor (precision ± 0.2 K) in a louvred radiation screen at 1.5 m above ground. One station was located in the town centre, with the sensor mounted on a post on the west side of a densely built commercial street, and two others were located amongst paddy fields and apple orchards several kilometres from the town centre. All data were stratified by month and season to help separate the variable effects of land cover, snow cover, soil wetness, and tree-canopy coverage on local air temperatures.

2.1.2. Vancouver, Canada

Vancouver is a modern city (population 2 million) with a high-rise core, low-density suburbs, an extensive urban forest, and a marine west coast climate. Temperatures were obtained from evening automobile traverses conducted in 1999, 2008, and 2010 (Oke, Christen). An instrumented vehicle was used to gather temperatures along a traverse route covering all major land uses in and around the city. The 1999 route differed slightly in length and number of observation points from 2008 and 2010. Temperatures were recorded with a copper-constantan thermocouple (precision ± 0.2 K) housed and ventilated in a PVC tube 1.5 m above ground. All traverses were conducted 3–5 h after sunset and required 2 h to complete.

Sites were preferentially selected along the traverse route to minimize elevation differences and to avoid shorelines, steep slopes, depressions, and other local relief features likely to cause thermal anomalies. The selection process ensured that source areas around the sites (within a radius of 200 m) were reasonably uniform in surface structure, land cover, and human activity. Topographic maps, aerial photographs, and reconnaissance surveys provided the necessary metadata to identify representative sites for LCZ classification. Hourly Φ_W values were calculated with synoptic weather data from Vancouver International Airport for each traverse night, and averaged across a 5-h period from sunset until completion of the traverse. Vancouver Airport is located within 10 km of the traverse route.

2.1.3. Uppsala, Sweden

Uppsala is a compact city (population 100 000) with a dense mid-rise core, a sharp urban–rural divide, and a humid continental climate. Temperatures were extracted from Sundborg's classic 1951 heat island study, in which 207 automobile traverses are reported for all times of day. Only those traverses conducted between sunset and sunrise were used in this study. Sundborg's route covered 15 observation points and required less than 1 h to complete. The points were carefully sited to yield temperatures that he showed to be statistically representative of their local surroundings. All temperatures were measured with a platinum-wire resistance thermometer (precision ± 0.2 K) mounted inside a radiation shield which was attached to the side of an automobile roof, at 1.5 m above ground.

Additional temperature data for Uppsala were obtained from Taesler (1980), who installed a city-wide network of nine fixed meteorological stations, each placed in an area of characteristic land cover and building density. At the stations, thermographs were enclosed in standard meteorological screens, 1.5 m above ground. The white, louvred enclosures were either mechanically aspirated or ventilated by wind. Taesler operated his network intermittently for 1 year to coincide with steady-state radiation-type weather that favoured heat island formation. His meteorological stations were classified into LCZ classes using the same methods and metadata sources as those used for Sundborg's 1951 study.

3. Numerical modelling approach

3.1. Model combination

3.1.1. Background

A combination of numerical models was used to simulate the thermal behaviour of LCZ classes under controlled conditions, i.e. with identical synoptic/mesoscale atmospheric forcing for all LCZs. This permits comparison of temperatures across a much larger set of LCZ classes and range of land cover properties (i.e. wet *vs* dry ground) than is possible with observations. To appropriately represent the thermal climate of each LCZ class, models of surface and atmospheric (thermo)dynamics were coupled (Krayenhoff *et al.*, 2009; Krayenhoff and Voogt, 2010). Temperatures for LCZs C–G in the 'land cover' series (Figure 1) were modelled with the Oregon State University Coupled Atmosphere-Plant-Soil (OSU-CAPS) scheme (Ek and Mahrt, 1991). LCZs A (*dense trees*) and B (*scattered trees*) were excluded from the modelling because OSU-CAPS is not suitable to simulate the effects of trees on surface thermal climate. OSU-CAPS consists of a soil-vegetation scheme (Mahrt and Pan, 1984; Pan and Mahrt, 1987) coupled to a one-dimensional atmospheric boundary layer model (Troen and Mahrt, 1986). OSU-CAPS is widely used and has been updated by several authors. Temperatures for all classes in the 'built' series (LCZs 1–10) were modelled with the atmospheric portion of the OSU-CAPS model coupled to the Town Energy Balance (TEB) urban surface scheme (Masson, 2000). The version of TEB used here has been evaluated and updated by Masson *et al.* (2002) and Lemonsu *et al.* (2004). When coupled, these surface–atmosphere models provide a simple but complete representation of heat, moisture, momentum, and radiation exchange between the surface and atmosphere above each LCZ class (Figure 2).

3.1.2. Atmospheric boundary layer model

Atmospheric dynamics for all LCZ classes were modelled with the OSU-CAPS boundary layer scheme (Figure 2). OSU-CAPS simulates the one-dimensional (i.e. vertical) mixing of heat, moisture, and momentum through the atmospheric boundary layer, ensuring that these quantities are appropriately distributed in the vertical. The scheme computes boundary layer eddy diffusivities following a non-local approach, i.e. based on surface layer velocity scales and diagnosed boundary layer height

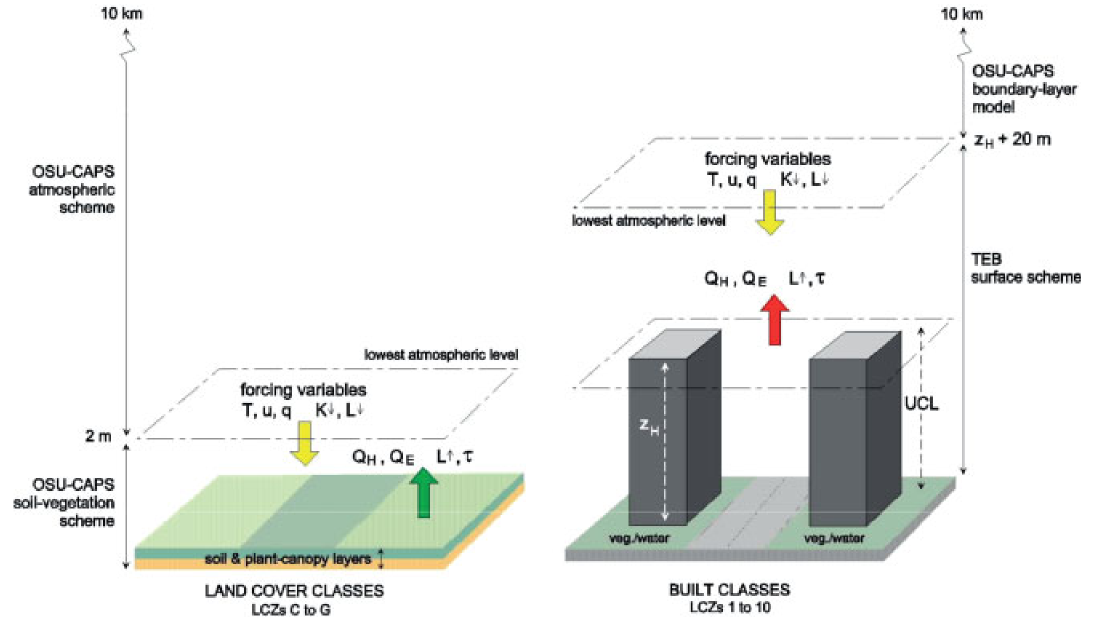

Figure 2. Schematic representation of the coupled OSU-CAPS and TEB models to simulate diurnal temperature range of LCZs. Symbol quantities: T = temperature, u = horizontal wind speed; q = humidity; Q_H = sensible heat flux density; Q_E = latent heat flux density; L↓ = incoming longwave radiation; L↑ = outgoing longwave radiation; K↓ = incoming shortwave radiation; K↑ = outgoing shortwave radiation, τ = momentum flux; z_H = height of roughness elements; UCL = urban canopy layer. Block arrows indicate variables that are passed between models.

(Ayotte *et al.*, 1996). It further adds a counter-gradient (enhancement) term for non-local transport of scalars during convective conditions. A prescribed profile of synoptic-scale subsidence helps maintain a capping inversion at the top of the boundary layer, which restricts the boundary layer to realistic heights (Krayenhoff and Voogt, 2010).

The simple 5-band longwave radiation scheme of Roach and Slingo (1979) is used to compute longwave heating/cooling in the atmosphere, and was coupled with the boundary layer model at each time step. Similarly, a shortwave radiation scheme, based on Bird and Hulstrom (1981), as presented in Iqbal (1983), was used to parameterize more robustly the direct and diffuse solar radiation reaching the surface. Simulations must represent the complete daily cycle of each LCZ class to capture differences in nocturnal cooling; hence, correct daytime solar irradiance is critical.

3.1.3. *Soil-vegetation model*

The soil-vegetation components of OSU-CAPS represent the interactions of three soil layers and a single plant-canopy layer (Figure 2). Together they quantify the surface–atmosphere and subsurface exchanges of heat, moisture, and radiation. The same model was used to estimate the thermal climate of LCZ G (*water*) (see Appendix A1).

3.1.4. *Urban model*

The TEB model parameterizes the surface energetics of a non-vegetated street canyon (Figure 2). TEB partitions a conceptualized canyon into three component surfaces: roads, roofs, and walls. Each component has its own thermal and radiative properties, surface and substrate temperature regimes, and surface energy budget. Buildings are identical and of simple shape, and roads (canyons) are of non-specific orientation (i.e. averaged over all directions). A full suite of physical processes is represented within this simplified geometry, including long- and shortwave radiation exchange (shading/trapping), latent and sensible turbulent heat fluxes, heat storage uptake and release, and basic urban hydrology (Masson, 2000).

TEB includes water and snow reservoirs on roofs and roads. Tests of the snowmelt submodel in TEB show good performance for roofs and alleys, but less so for roads (Lemonsu *et al.*, 2010). Methods to simulate trees in urban canyons are not available in TEB. Therefore, snow-cover and treed-canyon simulations were excluded from the TEB modelling of LCZs. However, canyon surface-vegetative cover (e.g. grass) was included, such that the road was assumed to be covered by water over a surface fraction equal in area to that vegetated (i.e. pervious) for each LCZ class (Appendix A1).

3.1.5. *Coupled model operations*

Temperature, humidity, and wind speed at the lowest atmospheric level, as well as direct and diffuse incoming shortwave radiation and downward longwave radiation, were input to the relevant surface scheme (i.e. TEB, or the soil-vegetation portion of OSU-CAPS). The lowest atmospheric level was 2 m for LCZs C–G, and 20 m above rooftop for all other zones. The surface scheme returned sensible heat, latent heat, longwave radiation, and momentum fluxes to the boundary layer scheme, which mixed heat, moisture, and momentum throughout the boundary layer and updated the temperature, wind, and humidity values at each atmospheric level. Atmospheric temperatures at these levels were further adjusted according to the cooling from the longwave scheme.

3.2. Simulation setup

Model simulations for each LCZ class were run for two surface-moisture states: wet and dry. Parameters input to TEB (for 'built' LCZ classes) and OSU-CAPS (for 'land cover' classes) are tabulated and discussed in Appendix A2 (Tables A2.1 and A2.2). The cloud formation submodel of OSU-CAPS was switched off and the large-scale pressure gradient was held weak and constant, which is typical of fair weather. A weak advection term was added to the boundary layer model to approximate synoptic/mesoscale advection (Appendix A1).

All simulations were initialized with idealized atmospheric profile data derived from radiosonde measurements near Basel, Switzerland (47.6°N), on 30 May 2002 at 0000 hours. Simulations continued for a period of 84 h with 60-s time steps for all LCZ classes and for both wet and dry scenarios. At the start of each simulation, the models experienced 'spin-up' effects as the initial state of the system adjusted to the model forcing. To avoid these effects, the first ≈40 h of output from each simulation were discarded.

4. Results

The following sections give temperature differences between selected LCZ classes. In each of the three test cities, heat island magnitude is used to express these differences, and is defined as an LCZ temperature differential, i.e. $\Delta T_{\mathrm{LCZ\ X-Y}}$. Heat islands defined this way are not necessarily 'urban-centred' or 'island-like' in configuration: $\Delta T_{\mathrm{LCZ\ 3-D}}$, for example, expresses a temperature difference between two local-scale settings – *compact low-rise* and *low plants* – neither of which is necessarily 'urban' or 'rural', and together which may not form an island-like pattern. LCZs thereby reveal important differences of scale between the heat island effect and the local climates which comprise it. Additionally, LCZs provide a standard framework from which to base inter-city comparisons of heat island magnitude, and to substantiate those comparisons with climatologically relevant surface properties. Diurnal temperature range (DTR) is similarly used to express LCZ thermal differences, and to aid comparability of the modelled and observed data. For the observed data, DTR is defined as the difference between the daily maxima and minima, and for the modelled data, as the average temperature range over the final two diurnal cycles of a simulation (i.e. two heating periods and two cooling periods). While it is preferable to compare hourly LCZ temperature differences between the observed and modelled datasets, hourly model temperatures are not comparable among LCZ classes due to the divergence of LCZ thermal states after appropriate spin-up time in a (1D) column model.

4.1. Nagano, Japan

Ten observation sites were selected from the mobile surveys of Sakakibara and Matsui (2005) for classification into LCZs (Table 2). Thirty-two of 90 traverses met the required weather criteria. The traverses were stratified into three seasons to correspond with observed changes in rural soil cover and moisture regimes: (1) flooded rice fields (May–June), (2) drained, snow-free fields (December–March), and (3) drained, snow-covered fields (December–January). Temperatures in LCZs D (*low plants*) and B (*scattered trees*) are strongly influenced by seasonal change in soil cover, field wetness, and tree-canopy coverage. Heat island magnitudes defined by these zones also change with season (Figure 3). Marked changes in heat island magnitude occur in spring/summer (i.e. May–June) when fields are flooded for rice planting and tree-canopy coverage increases with leaf emergence.

The fixed stations in and around Obuse town were classified into LCZs 3 (street canyon), B (orchards), and D (rice fields). The street canyon site was difficult to classify because the canyon itself is *compact low-rise*, but the local surroundings are *open low-rise*. LCZ 3 was chosen as the best-fit class for this site. Trends in DTR and heat island magnitude among the Obuse stations further differentiate the LCZ classes. DTR is strongly influenced by seasonal flooding (spring) and draining (late summer) of the rice fields (Figure 4(a)). From September to mid-May, the DTR of LCZ D is at times more than 5 K greater than LCZ 3 because daily minima in the street canyon are higher than those in the drained fields. In spring/summer, differences in DTR between LCZ D_w (subscript w denotes 'wet,' see Figure 1) and LCZ 3 turn positive, meaning that DTR is less in the countryside than in the town centre. This reversal coincides with annual flooding of the rice fields. Heat island magnitudes follow the same cycle, increasing when rural fields are dry or drained, and decreasing when irrigated. The thermal effects of leaf emergence are also seen in the annual march of heat island magnitudes, and in the DTRs of LCZ B compared to the treeless LCZ 3 (Figure 4(b)).

4.2. Vancouver, Canada

The nocturnal temperature profile for 4 November 1999, a night with clear skies and low wind speeds, shows strong thermal patterns across Vancouver (Figure 5). Temperatures rise and fall as the traverse changes elevation and location. In LCZ 1, temperatures are 5–7 K higher than LCZ D, giving rise to a heat island ($\Delta T_{\mathrm{LCZ\ 1-D}}$) of about 6 K. As the traverse moves from LCZ 1 (city centre) to A (forested park), temperatures drop by 4 K, and from LCZ 6 (residential neighbourhood) to D (cropped fields), by a

Table 2. Metadata for Sakakibara and Matsui's (2005) mobile observation sites in Nagano, 2001–2002.

Site number	Classification	Photographs Eye level	Properties[a]	
1	 LCZ 2_4: *compact mid-rise* with *open high-rise*	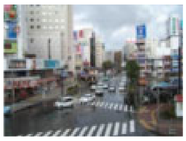	SVF % Built-up z_H	0.7 >95 20–30
2	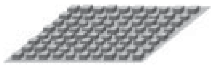 LCZ 3: *compact low-rise*	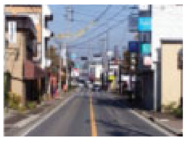	SVF % Built-up z_H	0.6 80 7
3, 4	 LCZ 6 : *open low-rise*		SVF % Built-up z_H	0.8–0.9 55 5
5, 6	 LCZ D: *low plants*		SVF % Built-up z_H	>0.9 <5 <1
7–10	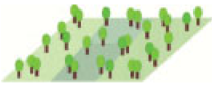 LCZ B: *scattered trees*		SVF % Built-up z_H	0.6–0.7 <5 3

[a]SVF = sky view factor (in summer); % Built-up = impervious surface fraction + building surface fraction; z_H = geometric average of building or plant-canopy heights (m).

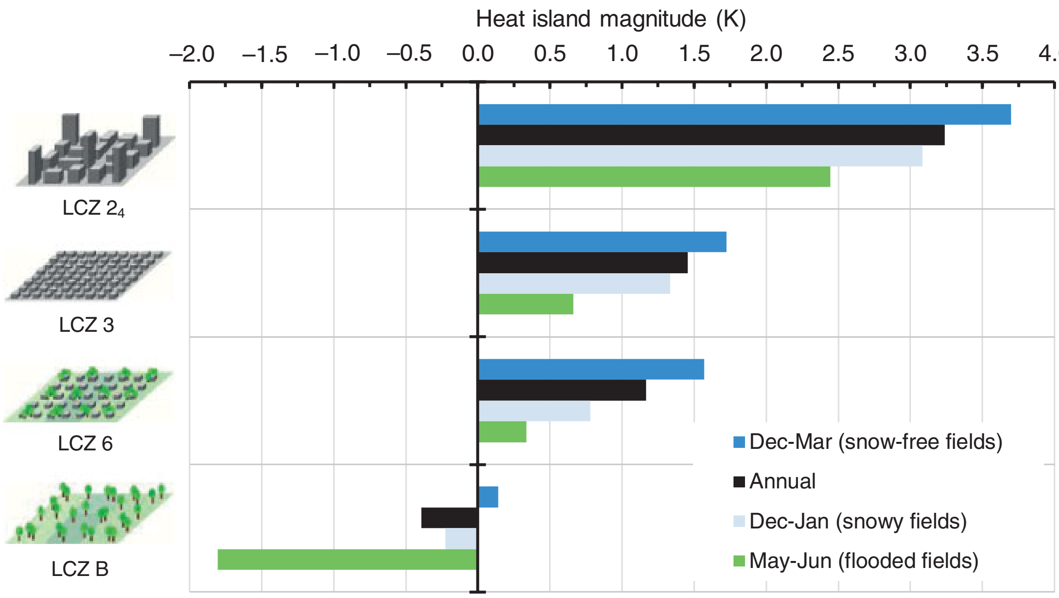

Figure 3. Heat island magnitude ($\Delta T_{\mathrm{LCZ\ X-D}}$) in Nagano basin during nighttime traverses, 2001–2002. LCZ D (Table II) is the baseline reference in all cases. Annual = 32 nights; May to June = 5 nights; December to March = 9 nights; December to January = 3 nights. Standard deviations for all bars are <1.2 K.

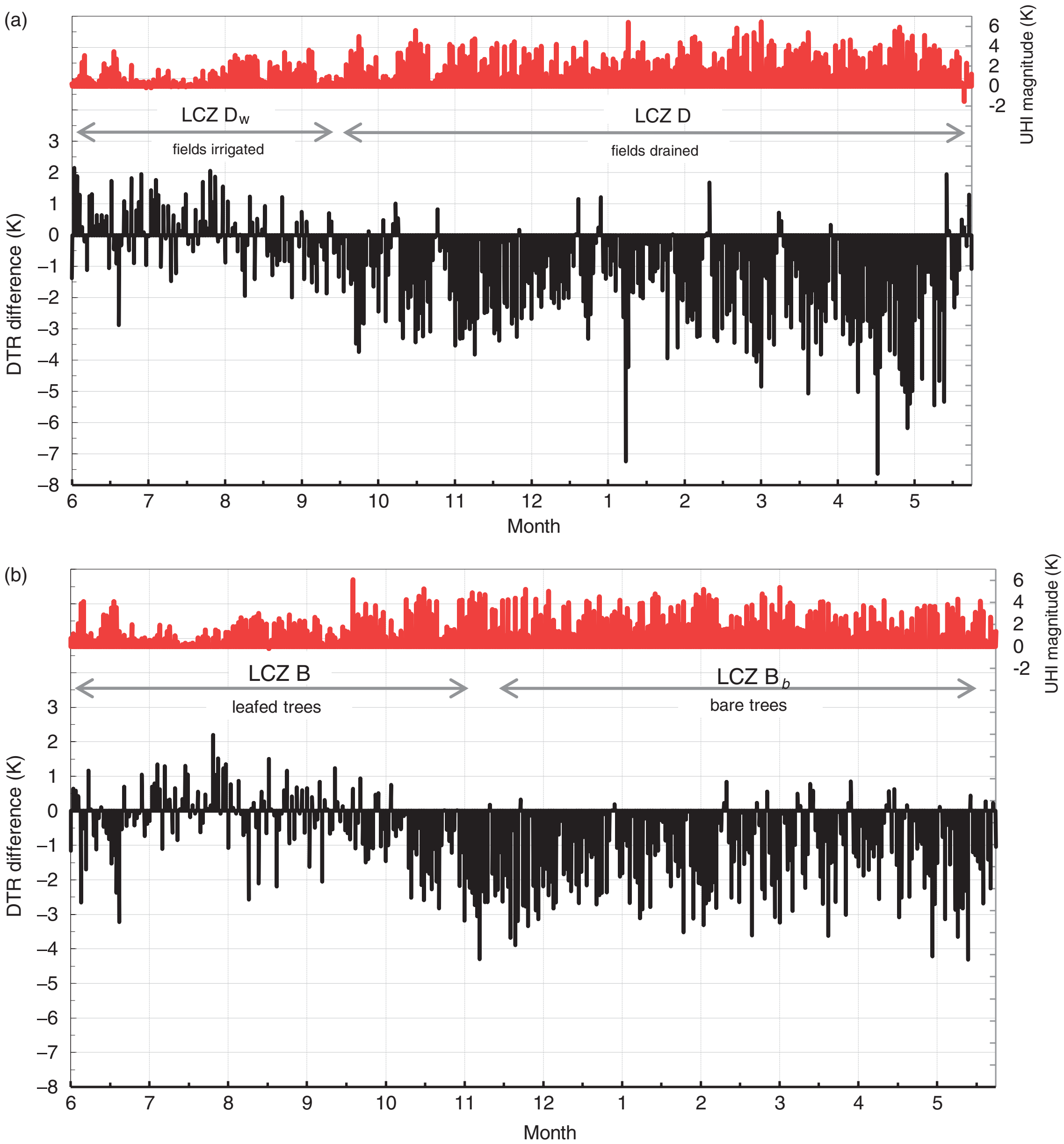

Figure 4. Differences in the diurnal temperature range (DTR) for local climate zones in Obuse town, 2006–2007. Daily heat island magnitudes (0000 hours) are shown across top of each graph. (a) LCZ 3 minus LCZ D; subscript *w* denotes ‘wet.’ (b) LCZ 3 minus LCZ B; subscript *b* denotes ‘bare trees’.

further 5 K. Heat island magnitude can be expressed by these zone combinations, e.g. $\Delta T_{\mathrm{LCZ\ 6-D}}$ and $\Delta T_{\mathrm{LCZ\ 1-A}}$ (Figure 5). However, within each LCZ, temperatures ‘dip’ and ‘spike’ as the micro-scale surroundings change (Figure 6). Traffic flow, building density, surface relief, and surface cover are not uniform in any LCZ, and thus temperatures fluctuate across short distances (10s of metres). It is therefore essential that heat island investigators use spatially averaged temperatures, or temperatures from sites known to be representative of the local surroundings, to quantify a meaningful heat island magnitude. The range of possible values (e.g. Figure 6) can otherwise yield erroneous heat island magnitudes (over- or under-estimates) and meaningless inter-city comparisons.

Of the 16 mobile traverses conducted in 2008 and 2010, only 4 passed the Φ_W weather filter. Sixteen sites along the traverse route were classified into LCZs (Table 3). Two sites in each LCZ class were plotted separately so as to regulate the topoclimatic effects of Vancouver’s coastal mountain setting (Figure 7). Each pair is similar in building/tree height and density, but slightly different in local relief, elevation, and/or vegetative cover. Within most LCZ pairs, temperature differences between control sites are <0.5 K, and between successive zones 0.5–2 K. This suggests that topoclimatic effects have been sufficiently controlled through site selection, and that the thermal effects of surface structure, land cover, and human activity are the primary cause of the observed temperature differences and heat island magnitudes.

Figure 5. Heat island magnitudes ($\Delta T_{\mathrm{LCZ\ X-D}}$) for Vancouver during a nighttime traverse in calm, clear weather (2200 hours; 4 November 1999). Thick horizontal lines indicate the distance travelled through, and the average temperature in, the LCZs of Vancouver. Surface relief and building height/density are shown along bottom axis.

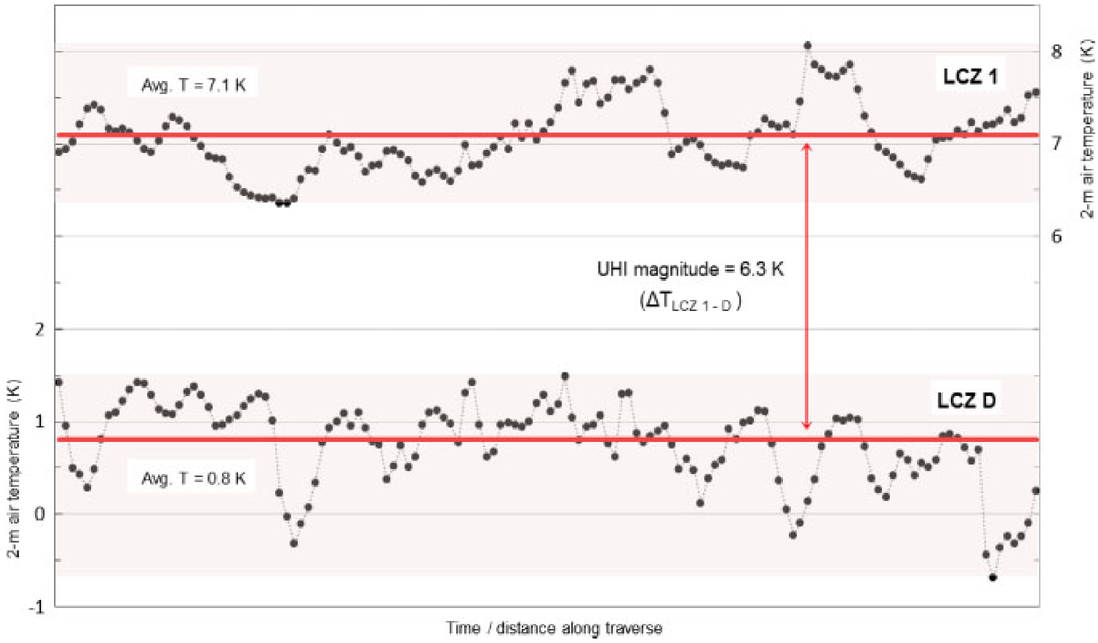

Figure 6. Temperature profiles for LCZs 1 and D in Figure 5. Temperatures were measured at 4-s intervals at an average automobile speed of 8–10 m s^{-1}. Standard deviations are 0.4 K for LCZ 1 and 0.5 K for LCZ D.

4.3. Uppsala, Sweden

Thirty-one nighttime traverses from Sundborg's (1951) heat island study met the weather criteria. The traverses were classified into three seasons: 'warm' (May to September), 'cold' (October to March), and 'snow' (days with snow cover >5 cm). Four observation sites were classified into LCZs (Table 4). In LCZ 2 (*compact mid-rise*), temperatures are 3–5 K higher than LCZ D; in LCZ 5 (*open mid-rise*), they are 2–3 K higher (Figure 8). Seasonal effects on LCZ thermal differences and heat island magnitudes are most obvious in the snow season. Regardless of LCZ class, heat island magnitudes are greatest when the ground is snow-covered. To further differentiate the local climates of Uppsala, four of Taesler's (1980) nine meteorological stations were classified into LCZs (Table 5). The period from 20 to 23 September 1976 was selected for its calm winds and clear skies. These conditions, combined with thermally responsive soils and a large daytime heat store in the urban fabric, are ideal for heat island formation and LCZ differentiation (Figure 9).

4.4. Numerical models

DTRs for all modelled LCZs represent two-day averages extracted from the daily near-surface temperature profiles

Table 3. Metadata for mobile observation sites in Vancouver, 2008 and 2010.

Site number	Classification	Photographs		Properties[a]	
		Eye level	Sky view		
1, 2	 LCZ 1: *compact high-rise*			SVF % Built-up z_H	0.20–0.25 >95 75–100
3, 4	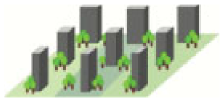 LCZ 4: *open high-rise*			SVF % Built-up z_H	0.5–0.55 80–85 30–50
5, 6	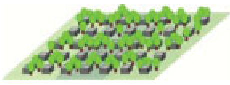 LCZ 6_A: *open low-rise* with *dense trees*	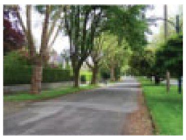		SVF % Built-up z_H	0.40–0.45 40–55 7–15
7, 8	 LCZ 8: *large low-rise*		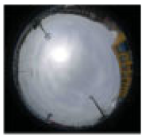	SVF % Built-up z_H	0.75 >95 5
9, 10	 LCZ 9: *sparsely built*			SVF % Built-up z_H	0.75–0.85 15–30 5
11, 12	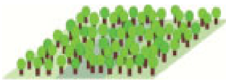 LCZ A: *dense trees*	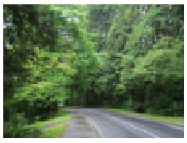	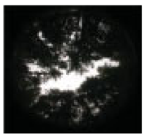	SVF % Built-up z_H	0.15–0.35 <10 15–25
13, 14	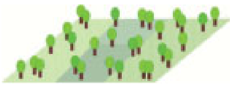 LCZ B: *scattered trees*	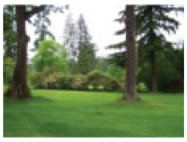		SVF % Built-up z_H	0.55–0.65 <10 5–10
15, 16	 LCZ D: *low plants*			SVF % Built-up z_H	0.85–0.90 <10 <1

[a]SVF = sky view factor (in summer); % Built-up = impervious surface fraction + building surface fraction; z_H = geometric average of building or plant-canopy heights (m).

of the OSU-CAPS and TEB schemes. To aid comparison with the observational data in Nagano, Vancouver, and Uppsala, the same baseline class (LCZ D: *low plants*) is used. The DTR for each class is therefore presented as a departure from the DTR for LCZ D_d (Figure 10). DTRs among the modelled LCZ classes range from 2.2 K in LCZ G (*water*) to 20.2 K in LCZ C_d (*bush, scrub* with *dry ground*). LCZ E (*bare rock or paved*) has no 'wet' DTR value because its impervious surface fraction is 1; similarly, LCZ G has no 'dry' value because its surface is wet by definition.

5. Discussion

5.1. Interpretation of the results

Observed temperatures in the LCZs of Nagano, Vancouver, and Uppsala should be viewed with the inherent challenges of an automobile traverse in mind. Traverses are

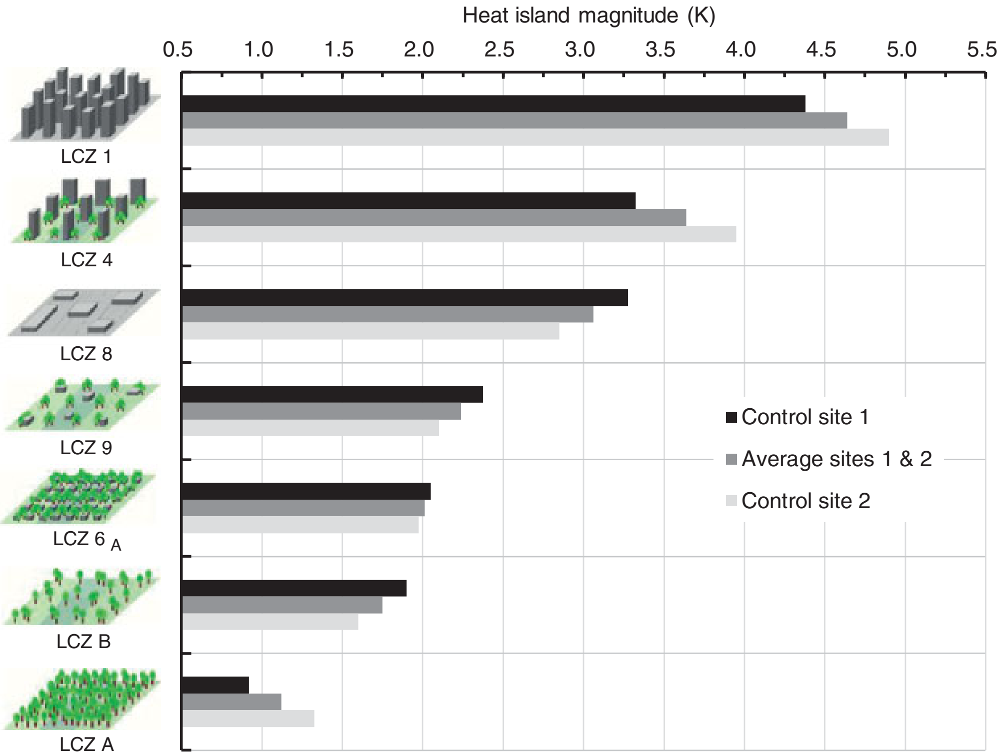

Figure 7. Heat island magnitude ($\Delta T_{\mathrm{LCZ\ X-D}}$) in Vancouver during nighttime traverses, March 2008 and 2010 (4 nights). Standard deviations are <1 K for all bars except LCZ A (<2 K).

biased because temperatures are measured above paved roads and at sites only accessible to cars. The micro-scale ($<10^2$ m) surface cover and exposure of these sites may not be representative of local scale (10^2 to 10^4 m) conditions (e.g. Figure 6). In Vancouver, temperature measurements in LCZ A (*dense trees*) were taken above asphalt roads and beneath openings in a dense tree canopy, conditions that, strictly, are not representative of that zone. Furthermore, since all automobile measurements were taken over the same surface cover (i.e. asphalt) at all LCZ sites, inter-zone temperature differences are likely underestimated.

Atmospheric numerical models are also subject to error and over-simplification. It is thus important to emphasize key model assumptions, as well as the range of scenarios for which a particular model is expected to be most reliable. First, temperatures simulated by TEB are representative of mid-canyon height – up to 20 m above ground in some LCZ classes – whereas temperatures from OSU-CAPS are representative of 2 m above ground. DTRs computed by TEB are therefore likely to be slightly smaller than actual values at 2-m height. This effect should be minor in most cases because canyon air is generally well mixed (Nakamura and Oke, 1988). Second, two different surface–atmosphere exchange schemes with different underlying assumptions and parameterizations were used to simulate LCZ temperatures. Most critically, 'wet' and 'dry' surfaces were defined and specified differently in the two models. The effects of this difference were mitigated by ensuring that the Bowen ratio values in LCZs 9 (TEB) and D (OSU-CAPS) were approximately equivalent. Third, TEB is designed for simple, dense, non-vegetated canyons, like those represented by LCZs 2 and 3. TEB is less appropriate for classes with abundant vegetation, high-rise buildings, and/or low aspect ratios like in LCZs 4, 8 and 9.

5.2. Generalizing the results

Overall, the results of this study support the divisional structure of the LCZ system. Among observational datasets, surface structure and land cover essentially drive thermal differences. During calm and clear evenings, thermal contrasts vary sympathetically with differences in pervious surface fraction and building/tree height and density. Thermal contrasts between zones with large differences in surface structure and cover, such as LCZs 1 and D (or 2 and D), can exceed 5 K. Thermal contrasts between zones of lesser difference, such as LCZs 9 and D (or B and D), are generally $\leq$2 K. These patterns are easily disrupted by the diurnal, seasonal, and topoclimatic effects of surface relief, surface wetness, tree cover, snow cover, and anthropogenic heat output, all of which can override or offset the immutable effects of building morphology and/or pervious surface fraction. For this reason relative temperature differences can vary between the same or similar LCZ pairs in different cities. Several LCZ classes show almost no thermal differences, which may be due to tree cover effects overriding building or land cover effects.

Table 4. Metadata for Sundborg's (1951) mobile observation sites in Uppsala, 1948–1949.

Site number	Classification	Photographs: Eye level	Photographs: Sky view	Properties[a]	
1	 LCZ 2: *compact mid-rise*		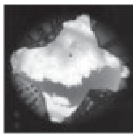	SVF % Built-up z_H	0.51 >95 10–15
2	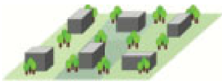 LCZ 5: *open mid-rise*		—	SVF % Built-up z_H	— 50 10
3	 LCZ 9: *sparsely built*	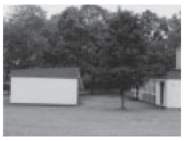	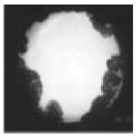	SVF % Built-up z_H	0.7 15 5–10
4	 LCZ D: *low plants*		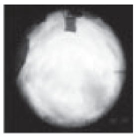	SVF % Built-up z_H	> 0.9 < 5 < 1

[a]SVF = sky view factor (in summer); % Built-up = impervious surface fraction + building surface fraction; z_H = geometric average of building or plant-canopy heights (m).

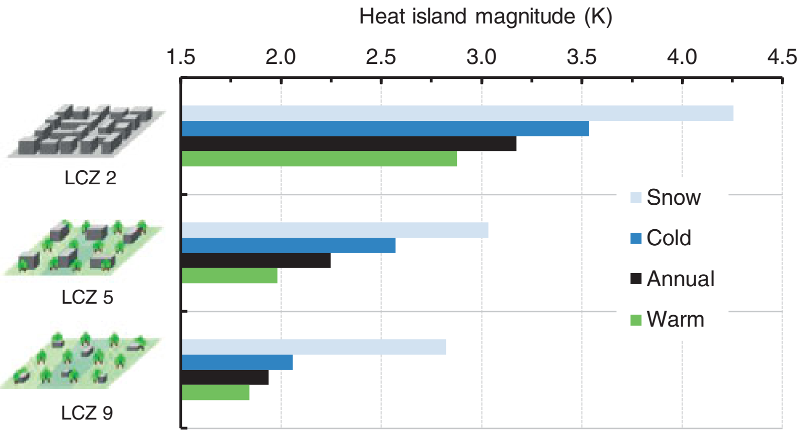

Figure 8. Heat island magnitude ($\Delta T_{\mathrm{LCZ\ X-D}}$) in Uppsala during nighttime traverses, 1948–1949 (*annual* = 31 nights; *warm* = 17 nights; *cold* = 14 nights; *snow* = 9 nights). Standard deviations for all bars are <2 K.

Nocturnal temperatures observed in compact built zones tend to be highest, followed by open and sparsely built zones, and lastly by treed and low plant zones. The two treed zones are warmer than the low plant cover zones, but cooler than the open built zones, although thermal differences between dense and scattered tree geometries are often negligible. Nocturnal temperatures drop by 1–3 K between compact and open built zones, and by another 1–3 K between open built and low plant cover zones, yielding a total differential across all zones of 3–6 K. The effect of snow cover on inter-zone thermal differences is difficult to isolate, due to limited snow-season data; in general, snow appears to increase nighttime temperature differences between built-up and natural zones by 0.5–1 K, as compared to snow-free differences. This increase is probably due to the (1) low thermal admittance, and therefore rapid nocturnal cooling, of snow surfaces in the countryside; (2) greater anthropogenic heat release in the city during the cold nights of the snow season; and (3) greater daytime heat storage in the urban area due to the removal of snow (high albedo) from city streets and parking lots.

These generalizations underpin our preference to express heat island magnitude through LCZ temperature differences. Defining the heat island magnitude in Vancouver as $\Delta T_{\mathrm{LCZ\ 1-D}} = 6\,\mathrm{K}$, Uppsala as

Table 5. Metadata for Taesler's (1980) meteorological stations in Uppsala, 1976.

Site number	Classification	Photographs		Properties[a]	
		Eye level	Sky view		
1	 LCZ 2: *compact mid-rise*			SVF % Built-up z_H	0.45 >95 15
2	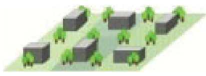 LCZ 5: *open mid-rise*			SVF % Built-up z_H	0.5 80 10
3	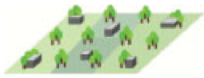 LCZ 9: *sparsely built*			SVF % Built-up z_H	0.7 20 5–10
4	 LCZ D: *low plants*			SVF % Built-up z_H	>0.9 <5 <1

[a]SVF = sky view factor (in summer); % Built-up = impervious surface fraction + building surface fraction; z_H = geometric average of building or plant-canopy heights (m).

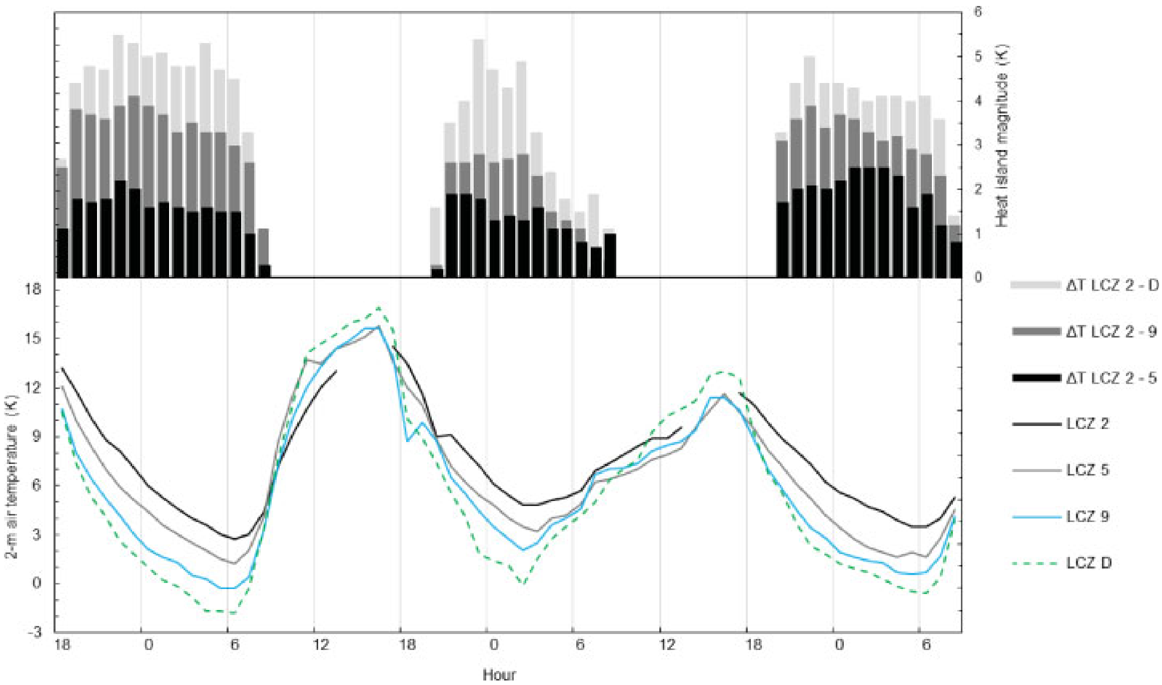

Figure 9. Heat island magnitude ($\Delta T_{\text{LCZ X-Y}}$) (*top*) and temperature-time series (*bottom*) for local climate zones in Uppsala, 20–23 September 1976 (*sunrise* = 0550 hours; *sunset* = 1815 hours). Afternoon temperatures for LCZ 2 are not shown due to erroneous values.

$\Delta T_{\text{LCZ 5-D}} = 3$ K, and Nagano as $\Delta T_{\text{LCZ 6-D}} = 1$ K makes explicit the local environments in which the temperatures were measured. Basic LCZ metadata (e.g. Figure 1, Table 1) convey that the reported heat island in Vancouver represents a landscape of densely packed high-rise buildings with little or no surface vegetation, whereas that of Uppsala represents an open landscape of mid-rise buildings and scattered trees, and of Nagano an open landscape of low-rise buildings and scattered trees. Because the LCZ classes in all three cities are paired to the same rural class (i.e. LCZ D), and variability in weather and surface relief conditions have been

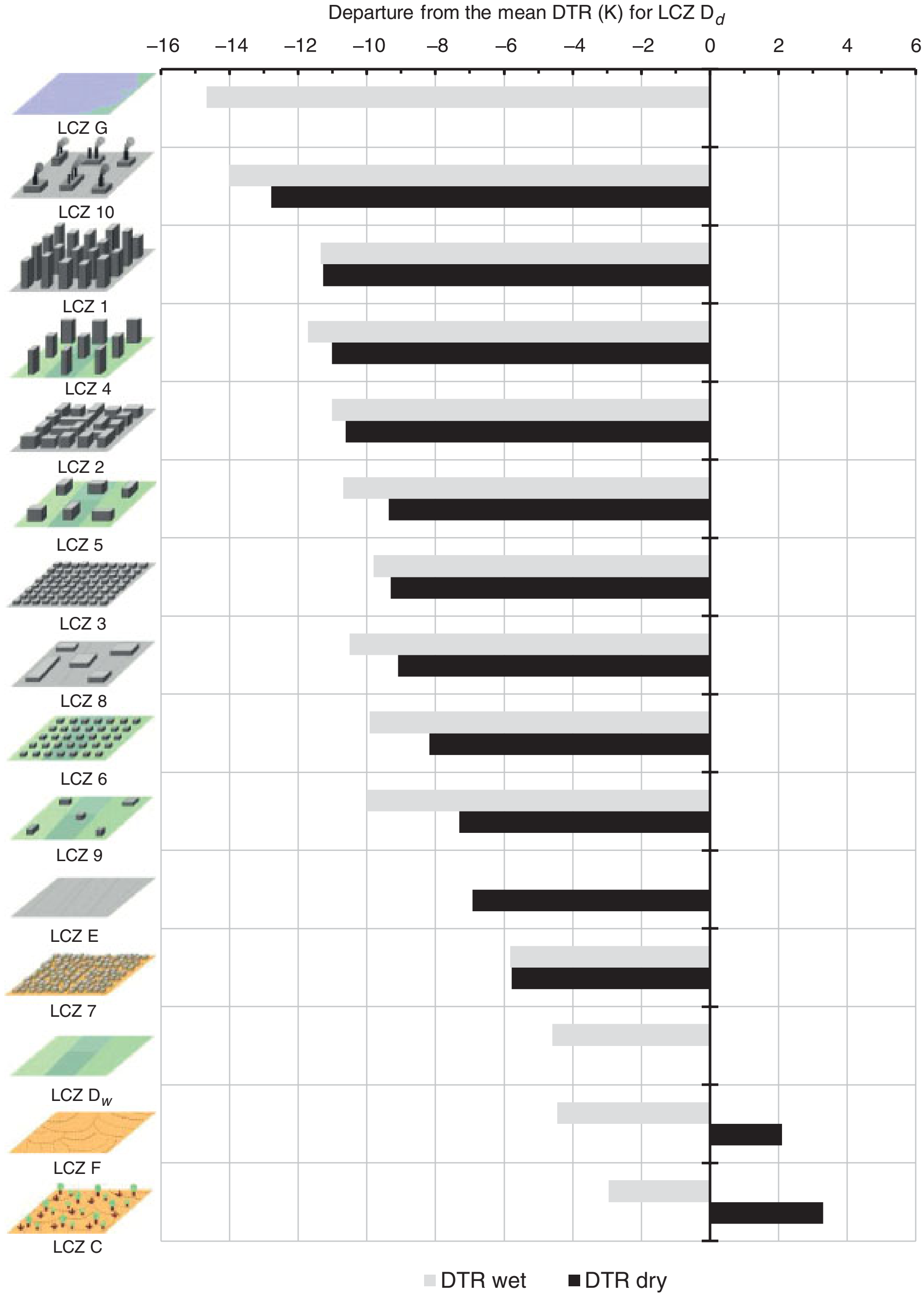

Figure 10. Simulated diurnal temperature range (DTR) for local climate zones. Trees are excluded from all zones. Mean DTR for LCZ $D_d = 17$ K.

controlled for through experimental design, validity of the comparisons is enhanced, physical explanation is given support, inter-city comparison is made quantifiable, and scientific exchange is clarified.

Among the modelled LCZ classes, DTRs vary with surface structure and land cover. LCZs composed of natural materials are more thermally responsive to daily heating (maxima) and cooling (minima) cycles than are those constructed of building materials. Compact and high-rise built forms are least thermally responsive, with DTRs of only 5–6 K, whereas natural zones (excluding *water*) are most responsive, with DTRs exceeding 16 K. The models clearly demonstrate the influence of pervious surface fraction and building height and spacing on DTR. An exception to this relation is LCZ 7 (*lightweight low-rise*), which, despite its compact form, has a relatively large DTR of 11 K. This is due to the low admittance of its lightweight construction materials. (We caution that no measured or published data are available in the literature to support the parameter values assigned to LCZ 7 in Appendix A2, Table A2.2.)

The modelling results further demonstrate that surface wetness significantly dampens DTR in LCZ classes with extensive pervious ground. This is probably because (1) wet soils have lower albedo and higher admittance than dry soils, and therefore greater capacity to absorb

Table 6. Comparison of modelled and observed diurnal temperature range (DTR)[a] in selected locations and local climate zones (LCZ).

Local climate zone	DTR modelled (K)	DTR observed (K)	Location	Data source
LCZ 1: compact high-rise	6	5–8	Vancouver, Canada	McClean (1993)
		6–9	Tokyo, Japan	Japan Meteorological Agency: http://data.jma.go.jp
LCZ 2: compact mid-rise	6	8–10	Goteborg, Sweden	Eliasson 1994
		11–15	Basel, Switzerland	Basel Urban Boundary Layer Experiment (BUBBLE): http://www.geog.ubc.ca/~achristn/research/BUBBLE
LCZ 3: compact low-rise	8	7–9	Kugahara, Japan	Kanda *et al.* 2005
LCZ 5: open mid-rise	8	10–12	Goteborg, Sweden	Eliasson 1994
		10–14	Uppsala, Sweden	Figure 9
LCZ 6: open low-rise	9	11–16	Uppsala, Sweden	Figure 9
		12–15	Vancouver, Canada	Environmental Prediction in Canadian Cities (EPiCC) Network: http://www.epicc.ca
LCZ 7: lightweight low-rise	11	10–14	Sao Paulo, Brazil	Silva and Ribeiro 2006
LCZ C: bush, scrub	20	17–23	Mohave, USA	Arizona Meteorological Network: http://ag.arizona.edu/azmet
LCZ D: low plants	17	10–15	Vancouver, Canada	McClean 1993
		15–18	Uppsala, Sweden	Figure 9
LCZ F: bare soil or sand	19	14–18	Basel, Switzerland	Basel Urban Boundary Layer Experiment (BUBBLE): http://www.geog.ubc.ca/~achristn/research/BUBBLE

[a]DTRs are representative of summer and/or dry season days with light winds and clear or partly cloudy skies.

and store heat; and (2) wet soils partition more energy into latent than sensible heat forms, thereby reducing daytime maxima. Surface wetness has slight or no effect in diminishing DTR in classes with little or no water storage potential, such as LCZs 1, 2, and 7. In the observational datasets from Nagano, daily extrema for LCZ D are diminished significantly by surface wetness.

Modelled DTR values for several LCZ classes show general agreement with observed values from other cities and datasets (Table 6). These data provide further support for the LCZ scheme in a wider context, and they confirm that the model results are reasonable. It is notable in this comparison that *modelled* DTR values are consistently lower than *observed* values for LCZs having an open form, a point that suggests TEB is less appropriate for these zones. Despite these discrepancies between and within the observed and modelled datasets, the most important finding in this study is that all LCZ classes are thermally unique, and all classes exhibit temperature contrasts that are largest at night, over dry surfaces, and in calm, clear weather.

6. Conclusions

The results here are the first to assess the thermal climates of LCZs. To the extent that these results show distinct thermal signatures of different zones, quantitative support is confirmed for the LCZ concept. The data used in this assessment originate from heat island observations in three mid-latitude cities, and from surface–atmosphere model simulations, all of which help substantiate the divisional structure of the LCZ scheme. LCZs are revealed to have unique thermal climates – under the limited relief and weather conditions tested in this study – that correspond with their surface structural and land cover characteristics. The division of urban and rural landscapes into LCZs is therefore justified on both physical and empirical grounds.

Also justified is the definition of heat island magnitude as an LCZ temperature difference, which facilitates communication and intercity comparison of results. This in turn helps heat island investigators to anticipate urban and rural thermal differences at the local scale, and to seek physical explanations for those differences. We encourage heat island investigators to extend testing of LCZs with more advanced numerical models, and with temperature observations from very different urban and rural environments than are utilized in this study. Further evaluation of LCZs will highlight changes to the scheme that are needed to more accurately classify the local thermal climates of cities and their countrysides.

Acknowledgements

We thank the following people for generously sharing unpublished datasets: Prof. Yasushi Sakakibara (Shinshu University, Nagano), Dr. Roger Taesler (SMHI, Norrköping), Dr. Andreas Christen (UBC, Vancouver), and the late Prof. Åke Sundborg (Uppsala University). We also thank the UBC Geography students who conducted temperature traverses in Vancouver in 1999, 2008, and 2010. The data and the accompanying field reports from these sources were essential to our evaluation of LCZs. This research is supported by a Discovery Grant to T.O. and Doctoral Fellowships to I.S. and S.K., from the Natural Sciences and Engineering Research Council of Canada.

Appendix: Model extension

A1.1. Atmospheric boundary layer model: advection

The 1D model simulations effectively represent each LCZ class as having no topography and infinite horizontal extent (horizontal homogeneity at local scales and larger). In reality, horizontal variation at these scales is always present, leading to variation in atmospheric boundary layer properties. These atmospheric gradients may generate winds themselves and may be advected by larger-scale (e.g. synoptic) circulations.

Model runs without advection develop unrealistically large day-to-day heating (or cooling) in the model column for many LCZ classes, in particular the more 'extreme' ones (e.g. LCZs 1 and 2), because longwave radiation escaping from the column top fails to approximately balance the solar radiation absorbed at the ground surface. Advection terms were therefore added to the prognostic equations for potential temperature and specific humidity (Krayenhoff and Voogt, 2010). Here, the strength of heat (moisture) advection was set proportional to the difference in temperature (humidity) between the current and initial profiles (with 12-hour relaxation period) under the assumption of static large-scale meteorological conditions. This ensured that day-to-day trends in modelled surface and atmospheric temperatures and humidities were realistic.

A1.2. Soil model: simulating LCZ G (*water*)

LCZ G (*water*) presents additional modelling challenges because water readily transmits solar radiation, and, being a fluid, is able to mix. As an alternative to adding yet another surface scheme to the overall simulation design, the OSU-CAPS soil model was adjusted to approximate the thermal response of an extensive body of water. Surface parameters such as albedo and roughness length were adjusted to appropriate values (Appendix A2, Table A2.1). To mimic vertical turbulent diffusion, the thermal conductivity was set to $80\,\mathrm{W\,m^{-1}\,K^{-1}}$ (higher values rendered the diffusion scheme unstable), which corresponds to a scalar diffusivity of $2.0 \times 10^{-5}\,\mathrm{m^2\,s^{-1}}$.

Table A2.1. Input parameter values for the soil-vegetation model (OSU-CAPS).

	Local climate zone (LCZ)				
	LCZ C Bush, scrub	*LCZ D* Low plants	*LCZ E*[a] Bare rock or paved	*LCZ F* Bare soil or sand	*LCZ G* Water
Pervious fraction	1.0	1.0	0	1.0	1.0
Albedo	0.25 Dry 0.20 Wet	0.25 Dry 0.25 Dry	0.2	0.28 Dry 0.18 Wet	0.06
Emissivity	0.93 Dry 0.98 Wet	0.91 Dry 0.93 Wet	0.95	0.93 Dry 0.98 Wet	1.0
Roughness length (m)	0.11	0.05	0.005	0.005	0.001
Thermal roughness length (m)	0.011	0.01	0.0025	0.0025	0.001
Soil type	Loamy sand	Loam	n.a.	Sandy loam	n.a.
Wilting point[b]	0.11	0.11	n.a.	n.a.	n.a.
Air dry values[c]	0.07	0.07	n.a.	0.07	n.a.
Reference value[d]	0.19	0.09	n.a.	n.a.	n.a.
Layer boundaries $d_1, d_2, \ldots, d_n$ (m)	0.05, 0.15 0.85	0.05, 0.15 0.85	n.a.	0.05, 0.15 0.85	0.25, 0.75 1.75, 3.75 7.75, 15.75
Volumetric soil moisture fraction	0.087 Dry 0.160 Wet	0.160 Dry 0.260 Wet	n.a.	0.124 Dry 0.212 Wet	n.a.
Height of roughness elements (m)	1.5	0.5	0	0.1	0
Minimum bulk stomatal resistance ($\mathrm{s\,m^{-1}}$)[e]	60	30	n.a.	n.a.	n.a.
Thermal admittance of ground ($\mathrm{J\,m^{-2}\,s^{-1/2}\,K^{-1}}$)[f]	800 Dry 1600 Wet	800 Dry 1600 Wet	2000	800 Dry 1600 Wet	n.a.[f]

[a]LCZ E was modelled with TEB; it is included in this table because it has no canyons (roofs, walls, roads) and no anthropogenic heat sources.
[b]Soil moisture fraction below which plants can no longer draw water from the soil.
[c]Surface soil moisture fraction below which direct evaporation ceases.
[d]Deep soil moisture fraction below which vegetation canopy transpiration is limited.
[e]Corresponds to the maximum rate at which water vapour may diffuse out of leaves.
[f]Heat capacity of water is $4.09\,\mathrm{J\,m^{-3}\,K^{-1}} \times 10^6$, and thermal conductivity is $80\,\mathrm{W\,m^{-1}\,K^{-1}}$ (to mimic vertical mixing).

Table A2.2. Input parameter values for the urban surface model (TEB).

Parameter	Local climate zone (LCZ)				
	LCZ 1 Compact high-rise	*LCZ 2* Compact mid-rise	*LCZ 3* Compact low-rise	*LCZ 4* Open high-rise	*LCZ 5* Open mid-rise
Land cover					
Building plan area fraction	0.5	0.5	0.55	0.3	0.3
Pervious surface fraction	0.05	0.1	0.15	0.35	0.3
Geometric					
Mean building height (m)	45	15	5	40	15
Mean canyon aspect ratio	2.5	1.25	1.25	1	0.5
Roof thickness (m)	0.3	0.3	0.2	0.3	0.25
Wall thickness (m)	0.3	0.25	0.2	0.2	0.2
Road thickness (m)	0.25	0.25	0.25	0.25	0.25
Aerodynamic					
Building roughness length, z_0 (m)	6.75	1.5	0.4	5.25	1.25
Displacement height, z_d (m)	27	10	4	23	6.9
Roof roughness length (m)	0.15	0.15	0.15	0.15	0.15
Road roughness length (m)	0.05	0.05	0.05	0.05	0.05
z_{0m}/z_{0h} [a]	200	200	200	200	200
Radiative					
Roof albedo	0.13	0.18	0.15	0.13	0.13
Wall albedo	0.25	0.2	0.2	0.25	0.25
Road albedo (dry, wet)[b]	0.15, 0.15	0.16, 0.15	0.18, 0.16	0.20, 0.17	0.20, 0.17
Roof emissivity	0.91	0.91	0.91	0.91	0.91
Wall emissivity	0.9	0.9	0.9	0.9	0.9
Road emissivity	0.95	0.95	0.95	0.95	0.95
Thermal					
Roof thermal admittance ($J\,m^{-2}\,s^{-1/2}\,K^{-1}$)	1500	1500	1200	1500	1500
Wall thermal admittance ($J\,m^{-2}\,s^{-1/2}\,K^{-1}$)	1400	2000	1600	1700	1700
Road thermal admittance (dry, wet)[c] ($J\,m^{-2}\,s^{-1/2}\,K^{-1}$)	1157	1106	1060	992	964
	1239	1287	1330	1397	1425
Other					
Anthropogenic heat flux density ($W\,m^{-2}$)	100	35	30	30	15
% To canopy layer	60	50	50	50	50
% To boundary layer	40	50	50	50	50

This value is at the low end of the diffusivity of oceanic tracers reported by Benitez-Nelson *et al.* (2000). Vertical layers were thicker and more numerous than in the other classes, extending down > 15 m. Assuming a moderate chlorophyll profile, the receipt of solar radiation no longer occurs at the surface but is distributed through all layers, according to the Ohlmann and Siegel (2000) model. For the present scenario, this indicated that 38 % of incoming solar radiation was absorbed in the uppermost 0.25 m, and 19% at depths >8 m. Finally, because surface spatial variability is lower over larger bodies of water as compared to land, the advection (relaxation) timescale was doubled. This produced more reasonable oceanic surface layer profiles (approximately neutral as opposed to stable).

A1.3. Urban model: simulating urban pervious surfaces

Standing water on the road was substituted for canyon vegetation as a simple adjustment to capture the atmospheric cooling effects (via latent heat) of surface plant cover. This approach aligns with other simple additions of vegetation effects in urban canopy models (e.g. Yaghoobian *et al.* 2010). The latent heat flux from the standing-water portion of the road, as modelled by TEB, was multiplied by a moisture availability coefficient of 1.0 for all 'wet' simulations and 0.1 for 'dry' simulations. Effective thermal and radiative parameters for the 'road' in these 'vegetated' canyon simulations were derived by weighting appropriate values for the pervious/impervious surface fraction of each built landscape, following Salamanca *et al.* (2009). The weighted 'road' values of these parameters then differed between 'wet' and 'dry' simulations (Appendix A2, Table A2.1).

Appendix A2: Surface model parameters and inputs

The soil-vegetation surface in OSU-CAPS and the urban surface in TEB are quantified by geometric, radiative, thermal, and land cover parameters (Tables A2.1 and A2.2). A representative set of values for these parameters was compiled for each LCZ class. Values were retrieved from several sources, including terrestrial/aerial photographs; previous modelling studies using OSU-CAPS and TEB; general texts of physical climatology, remote sensing, and soil science; and the observational and modelling subliteratures of urban climatology.

Table A2.2. *(Continued)*

Parameter	Local climate zone (LCZ)				
	LCZ 6 Open low-rise	*LCZ 7* Lightweight low-rise	*LCZ 8* Large low-rise	*LCZ 9* Sparsely built	*LCZ 10* Heavy industry
Land cover					
Building plan area fraction	0.3	0.8	0.4	0.15	0.25
Pervious surface fraction	0.4	0.15	0.15	0.7	0.45
Geometric					
Mean building height (m)	5	3	7	5	8.5
Mean canyon aspect ratio	0.5	1.5	0.2	0.15	0.35
Roof thickness (m)	0.15	0.05	0.12	0.15	0.05
Wall thickness (m)	0.2	0.1	0.2	0.2	0.05
Road thickness (m)	0.25	0.25	0.25	0.25	0.25
Aerodynamic					
Building roughness length (m)	0.5	0.2	0.55	0.35	1.1
Displacement height (m)	3	2.5	4	2	5.5
Roof roughness length (m)	0.15	0.15	0.15	0.15	0.15
Road roughness length (m)	0.05	0.05	0.05	0.05	0.05
z_{0m}/z_{0h}[a]	200	200	200	200	200
Radiative					
Roof albedo	0.13	0.15	0.18	0.13	0.1
Wall albedo	0.25	0.2	0.25	0.25	0.2
Road albedo (dry, wet)[b]	0.21, 0.18	0.24, 0.20	0.17, 0.16	0.23, 0.19	0.21, 0.18
Roof emissivity	0.91	0.28	0.91	0.91	0.91
Wall emissivity	0.9	0.9	0.9	0.9	0.9
Road emissivity	0.95	0.92	0.95	0.95	0.95
Thermal					
Roof thermal admittance ($J\,m^{-2}\,s^{-1/2}\,K^{-1}$)	1200	2000	1500	1200	2000
Wall thermal admittance ($J\,m^{-2}\,s^{-1/2}\,K^{-1}$)	1600	600	1500	1600	1500
Road thermal admittance (dry, wet)[c] ($J\,m^{-2}\,s^{-1/2}\,K^{-1}$)	936	842	1094	866	953
	1454	1448	1297	1527	1437
Other					
Anthropogenic heat flux density ($W\,m^{-2}$)	10	30	40	5	300
% To canopy layer	40	50	40	50	20
% To boundary layer	60	50	60	50	80

[a]Ratio of momentum roughness length to heat roughness length for *surface*-atmosphere transfer.
[b]Road albedos are weighted by the impervious and pervious surface fractions of each LCZ. Impervious albedos are 0.14 for all zones except LCZ 7 (0.18); pervious values are 0.25 and 0.20 for all zones for dry and wet surfaces, respectively (see LCZ C and D; Table A2.1).
[c]Road thermal admittances are weighted by the impervious and pervious surface fractions of each LCZ. Impervious admittances are 1200 for all zones except LCZ 7 (1000); pervious values are 800 and 1600 for all zones for dry and wet surfaces, respectively (see LCZ C, D, and F; Table A2.1).

Anthropogenic heat flux (Q_F) from transportation and industrial sources is prescribed in TEB. The diurnal profile for Q_F in each LCZ class was scaled from the modelled values of Sailor and Lu (2004) for Chicago. The diurnal profiles are therefore biased to the values of a large North American city, but the low Q_F of most LCZ classes renders this effect minor. The exception to this scaling was LCZ 10 (*heavy industry*), whose diurnal profile was held constant.

Finally, TEB computes building internal heating/cooling implicitly with a building internal temperature that varies slowly according to external conditions and has a set minimum (Masson *et al.* 2002). However, in landscapes classified as LCZ 7 (*lightweight low-rise*), heating and air conditioning of structures is not common. Hence all building interior heating/cooling is removed for this zone, by setting the temperature gradient to zero at the inside edge of the building walls and roofs.

References

Aguilar E, Auer I, Brunet M, Peterson TC, Wieringa J. 2003. Guidance on Metadata and Homogenization. World Meteorological Organization, Geneva, WMO Technical Document No. 1186.

Ayotte KW, Sullivan PP, Andrén A, Doney SC, Holtslag AAM, Large WG, McWilliams JC, Moeng C-H, Otte MJ, Tribbia JJ, Wyngaard JC. 1996. An evaluation of neutral and convective planetary boundary-layer parameterizations relative to large eddy simulations. *Boundary-Layer Meteorology* **79**: 131–175.

Benitez-Nelson CR, Buesseler KO, Crossin G. 2000. Upper ocean carbon export, horizontal transport, and vertical eddy diffusivity in the southwestern Gulf of Maine. *Continental Shelf Research* **20**: 707–736.

Bird R, Hulstrom RL. 1981. A simplified clear sky model for direct and diffuse insolation on horizontal surfaces. Solar Energy Research Institute Technical Report SERI/TR-642-761, Golden, CO.

Bolz HM. 1949. Die abhangigkeit der infraroten gegenstrahlung von der bewolkung [The dependence of infrared radiation on clouds]. *Zeitschrift fur Metorologie* **3**: 201–203.

Ek M, Mahrt L. 1991. *OSU 1-D PBL Model User's Guide*. Department of Atmospheric Sciences, Oregon State University: Corvallis.

Eliasson I. 1994. Urban-suburban-rural air temperature differences related to street geometry. *Physical Geography* **15**: 1–22.

Iqbal M. 1983. *An Introduction to Solar Radiation*. Academic Press: New York.
Kanda M, Moriwaki R, Kimoto Y. 2005. Temperature profiles within and above an urban canopy. *Boundary-Layer Meteorology* **115**: 499–506.
Krayenhoff ES, Voogt JA. 2010. Impacts of urban albedo increase on local air temperature at daily through annual time scales: Model results and synthesis of previous work. *Journal of Applied Meteorology and Climatology* **49**: 1634–1648.
Krayenhoff ES, Stewart ID, Oke TR. 2009. Estimating thermal responsiveness of local scale climate 'zones' with a numerical modeling approach. In *Preprints, TR Oke Symposium & Eighth Symposium on Urban Environment*, January 11–15, Phoenix, AZ.
Lemonsu A, Grimmond CSB, Masson V. 2004. Modeling the surface energy balance of the core of an old Mediterranean city: Marseille. *Journal of Applied Meteorology* **43**: 312–327.
Lemonsu A, Bélair S, Mailhot J, Leroyer S. 2010. Evaluation of the Town Energy Balance model in cold and snowy conditions during the Montreal Urban Snow Experiment, 2005. *Journal of Applied Meteorology and Climatology* **49**: 346–362.
Mahrt L, Pan H-L. 1984. A two-layer model of soil hydrology. *Boundary-Layer Meteorology* **29**: 1–20.
Masson V. 2000. A physically-based scheme for the urban energy budget in atmospheric models. *Boundary-Layer Meteorology* **94**: 357–397.
Masson V, Grimmond CSB, Oke TR. 2002. Evaluation of the Town Energy Balance (TEB) scheme with direct measurements from dry districts in two cities. *Journal of Applied Meteorology* **41**: 1011–1026.
McClean A. 1993. *The Evaluation and Modification of a Prediction Model for Road Surface Temperatures*, MSc Thesis, University of British Columbia: Vancouver.
Mizuno M, Nakamura Y, Murakami H, Yamamoto S. 1990/91. Effects of land use on urban horizontal atmospheric temperature distributions. *Energy and Buildings* **15**: 165–176.
Nakamura Y, Oke TR. 1988. Wind, temperature and stability conditions in an E-W oriented urban canyon. *Atmospheric Environment* **22**: 2691–2700.
Ohlmann JC, Siegel DA. 2000. Ocean radiant heating. Part II: Parameterizing solar radiation transmission through the upper ocean. *Journal of Physical Oceanography* **30**: 1849–1865.
Oke TR. 1973. City size and the urban heat island. *Atmospheric Environment* **7**: 769–779.
Oke TR. 1998. An algorithmic scheme to estimate hourly heat island magnitude. In *Preprints, 2nd Urban Environment Symposium*, 2–6 November, Albuquerque, NM.
Oke TR. 2004. Initial guidance to obtain representative meteorological observations at urban sites. IOM Report No. 81, World Meteorological Organization. Geneva.
Oke TR. 2006. Towards better scientific communication in urban climate. *Theoretical and Applied Climatology* **84**: 179–190.
Pan H-L, Mahrt L. 1987. Interaction between soil hydrology and boundary-layer development. *Boundary-Layer Meteorology* **38**: 185–202.
Roach WT, Slingo A. 1979. A high resolution infra-red radiative transfer scheme to study the interaction of radiation with cloud. *Quarterly Journal of the Royal Meteorological Society* **105**: 603–614.
Runnalls KE, Oke TR. 2006. A technique to detect microclimate inhomogeneities in historical records of screen-level air temperature. *Journal of Climate* **19**: 959–978.
Sailor DJ, Lu L. 2004. A top-down methodology for determining diurnal and seasonal anthropogenic heating profiles for urban areas. *Atmospheric Environment* **38**: 2737–2748.
Sakakibara Y. 1999. The relationship between heat island intensity and rural land coverage in Obuse, Nagano. *Tenki* **46**: 567–575. In Japanese.
Sakakibara Y, Matsui E. 2005. Relation between heat island intensity and city size indices/urban canopy characteristics in settlements of Nagano basin, Japan. *Geographical Review of Japan* **78**: 812–824.
Salamanca F, Krayenhoff ES, Martilli A. 2009. On the derivation of material thermal properties representative of heterogeneous urban neighbourhoods. *Journal of Applied Meteorology and Climatology* **48**: 1725–1732.
Silva E, Ribeiro H. 2006. Temperature modifications in shantytown environments and thermal discomfort. *Revista de Saude Publica* **40**: 1–8.
Stewart ID. 2011a. A systematic review and scientific critique of methodology in modern urban heat island literature. *International Journal of Climatology* **31**: 200–217.
Stewart ID. 2011b. *Redefining the Urban Heat Island*, PhD Dissertation, University of British Columbia, Vancouver.
Stewart ID, Oke TR. 2012. 'Local climate zones' for urban temperature studies. *Bulletin of the American Meteorological Society* **93**: 1879–1900.
Sundborg Å. 1951. Climatological studies in Uppsala with special regard to the temperature conditions in the urban area. Geographica No. 22, Geographical Institute of Uppsala.
Taesler R. 1980. Studies of the development and thermal structure of the urban boundary layer in Uppsala. Report No. 61, Uppsala University Meteorological Institute.
Tanner CB. 1963. Basic Instrumentation and Measurements for Plant Environment and Micrometeorology. Soils Bulletin 6, Department of Soil Science, University of Wisconsin.
Troen IB, Mahrt L. 1986. A simple model of the atmospheric boundary layer: Sensitivity to surface evaporation. *Boundary-Layer Meteorology* **37**: 129–148.
Yaghoobian N, Kleissl J, Krayenhoff ES. 2010. Modeling the thermal effects of artificial turf on the urban environment. *Journal of Applied Meteorology and Climatology* **49**: 332–345.

